Smart Structures and Systems, *Vol. 29, No. 5 (2022) 661-675*
https://doi.org/10.12989/sss.2022.29.5.661

Improvement of the amplification gain for a propulsion drives of an electric vehicle with sensor voltage and mechanical speed control

Karim Negadi*[1], Mohamed Boudiaf [2], Rabah Araria [1] and Lazreg Hadji [3]

[1] *L2GEGI Laboratory, Department of Electrical Engineering, Faculty of Applied Science, University of Tiaret, BP 78 Zaaroura, 14000, Tiaret, Algeria*
[2] *Department of Electrical Engineering, Ziane Achour University of Djelfa, Djelfa, Algeria*
[3] *Department of Mechanical Engineering, University of Tiaret, BP 78 Zaaroura, Tiaret,14000, Algeria*

(*Received March 16, 2021, Revised August 11, 2021, Accepted January 27, 2022*)

Abstract. In this paper, an electric vehicle drives with efficient control and low cost hardware using four quadrant DC converter with Permanent Magnet Direct Current (PMDC) motor fed by DC boost converter is presented. The main idea of this work is to improve the energy efficiency of the conversion chain of an electric vehicle by inserting a boost converter between the battery and the four quadrant-DC motor chopper assembly. Consequently, this method makes it possible to maintain the amplification gain of the 4 quadrant chopper constant regardless of the battery voltage drop and even in the presence of a fault in the battery. One of the most important control problems is control under heavy uncertainty conditions. The higher order sliding mode control technique is introduced for the adjustment of DC bus voltage and mechanical motor speed. To implement the proposed approach in the automotive field, experimental tests were carried out. The performances obtained show the usefulness of this system for a better energy management of an electric vehicle and an ideal control under different operating conditions and constraints, mostly at nominal operation, in the presence of a load torque, when reversing the direction of rotation of the motor speed and even in case of battery chamber failure. The whole system has been tested experimentally and its performance has been analyzed.

Keywords: battery; DC boost converter; electric vehicle; four quadrant DC converter; higher order sliding mode control; mechanical speed and voltage control; sensor control of PMDC motor drives

1. Introduction

The transport sector is heavily dependent on the internal combustion engine because of its good driving range and short refueling time. However, due to the growing environmental awareness, alternatives which are not dependent on fossil fuel are being investigated. The battery-powered Electric Vehicle (EV) has been proposed as an alternative since it can recharge its batteries from renewable energy sources (such as wind power or solar cells). The simple design of the electric engine is another favorable factor, since it involves fewer moving parts than combustion engines usually require. The main issues of the EV are the driving range and the time required to recharge, which are dependent on the energy storage element (battery or supercapacitor) (Berigai Ramaiaha *et al*. 2018).

Batteries consist of electrochemical cells, and provide electrical energy through chemical reactions. Recharging is done by reversing said reactions. The internal processes in batteries are complex, different charge/recharge-cycles affect the performance and efficiency, there are limits to how fast the recharging can be done, etc. Typically, an EV requires several hours of grid connection before being fully recharged (Yang *et al*. 2014).

The battery provides DC current, but the motor/generator is a three-phase machine. Hence, a bidirectional AC-DC (inverter/rectifier) is used together with a DC-DC converter, which acts as a power valve. This report is focused on the latter, a 4-quadrant DC-DC converter, whose purpose is to control the amount of power and energy that is transferred between the flywheel and the battery (Dursun *et al*. 2017).

The DC-DC converter has specifications which differ from other converter structures, among these specifications: must be able to provide both higher and lower output voltage (step-down and step-up mode), must be bidirectional (battery charging in braking mode), must be able to control current, for battery charging and to stay within the motor winding limits, the control must be parameter invariant, it mean that the variations in input / output dynamics must not affect performance, control must be able to operate in all four quadrants and move transparently, voltages test devices should range between 0 and 50 volts, but the design should be scalable to higher voltages, power levels and the test current should be between 0 and 10 amps, but must also be scalable and must control the flow of power between the battery and the motor (Vasappa and Daykumar 2010). This technical solution to insert a DC boost regulator can be used to equip autonomous or non-autonomous electrical installations with

*Corresponding author, Professor,
E-mail: karim.negadi@univ-tiaret.dz

ISSN: 1738-1584 (Print), 1738-1991 (Online)

several hybrid photovoltaic sources, wind turbine, fuel cell and accumulator battery which allow energy to be stored and restore it in good time when meeting the needs of an electrical grid and a residential load (Khubalkar *et al*. 2017).

DC motors are used in many industrial applications like propulsion and electric traction due to the wide operating speed range. The speed control of Permanent Magnet Direct Current (PMDC) motors is achieved with less power loss by using switched power converters (Shi *et al*. 2019).

Since the PMDC motors have low inertia and fast response, they are suitable for applications such as process control, conveyors, pumps, winding machine etc. Speed regulation of PMDC motors with smooth dynamic response demands for non-linear and robust control schemes such as sliding mode, hybrid, adaptive, fuzzy and neural network.

Various control schemes are proposed for the speed regulation of PMDC motors in the literature. Artificial neural network based speed control is proposed and implemented for a PMDC motor to minimize the speed and current error in reference (Sankardoss and Geethanjali 2017). The proposed back propagation algorithm uses gradient minimization method to reduce the error. A sensor less speed control scheme is proposed in reference (Adel *et al*. 2018), in which error due to parameter variations is avoided by online parameter identification based on a recursive least square's estimation techniques. The speed, current and the current dynamic ripple errors are considered to design the controller for a 6 pulse converter fed PMDC motor is presented in references (Nagarajan *et al*. 2016).

The conventional linear control system design for PMDC motor drives consists of a properly tuned cascade configuration of PI speed and voltage controllers. Rather accurate information regarding the motor parameters and load conditions is necessary to guarantee the desired tradeoff between precision, bandwidth, and disturbance rejection. Unfortunately, several electromechanical parameters are not exactly known or subject to large variations during operation, leading to degradation of the drive performance (Hoyos *et al*. 2021).

The structure control schemes are typically based on control signals of the switching type, and the so-called "chattering" phenomenon, originated by the interaction between parasitic dynamics and high-frequency switching control, arises, which represents the most deleterious implementation drawback of this type of control.

The following works (Kiss *et al*. 2021, Saleem *et al*. 2020, Sankardoss and Geethanjali 2017) and references therein studied and analyzed the different control strategies, many investigations can be cited as examples of continuous and discrete-time nonlinear robust techniques for PMDC drives. Indeed, it solves the problem only partially, particularly when high dynamic performance is required, since the main characteristics of invariance and accuracy of the control systems are not assured any more.

Higher order sliding mode (HOSM) control technique is one of the robust control techniques and is widely used to design controller in many industrial applications, and it is successfully applied to switched power converters in Reference (Lavanya *et al*. 2012, Sankardoss and Geethanjali 2017).

This type of control makes it possible to avoid the complex adjustment of the proportional and integral gains of the conventional controller, and the adjustment can be done, in practice, by a few experimental / simulated tests where the gains of the controller are gradually increased according to the applied procedure.

Unless the conventional sliding mode technique, higher order sliding mode technique reduces the chattering effects and achieves any arbitrary reduced order dynamics on the sliding surface and its implementation is very simple. Sliding mode control technique is also used to regulate the speed and DC voltage of PMDC motors. Second-order sliding mode controllers are proposed for speed regulation of the PMDC motor in detail in Reference (O'Brien *et al*. 2014). In Reference (Tun and Naing 2018), the authors proposed a cascade control of a PMDC motor using second order sliding mode controller in which a current inner loop is used to control the speed for various load conditions (Hernández-Márquez *et al*. 2018).

The paper is organized as follows: section 2 presents a description review of the analyzed process. The physical modeling with their model of the motor equations used in the propulsion chain of the proposed electric vehicle is defined in the sections 3. In Section 4, the proposed control schemes for the DC boost converter and the PMDC mechanical motor are presented respectively. The description of the experimental test bench has been developed in Section 5. The experimental results and interpretation are presented in Section 6. Section 7 summarizes the work carried out in the conclusion.

2. A description review of the analyzed process

In order to improve the energy efficiency and to solve the problem of insufficient direct voltage in the conversion chain of an electric vehicle, generally three solutions are proposed (Bagheri *et al*. 2018): the first method is to insert a larger battery bank, it is a very expensive solution that requires a lot of maintenance and a lot of space (Fig. 1). The second method introduce an adaptive control in order to update the parameters of regulators, this method becomes more and more ineffective in the case of a significant

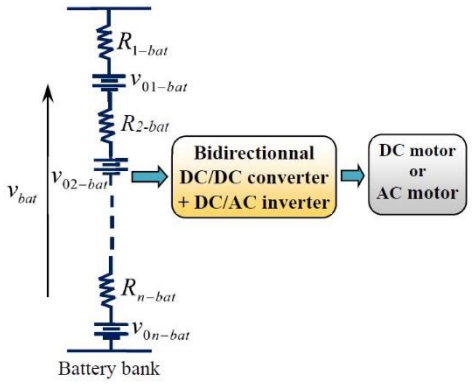

Fig. 1 Improved energy efficiency by re-coupling several battery units in series

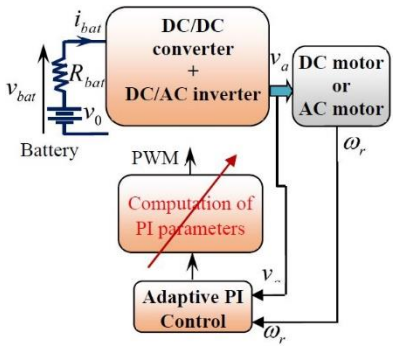

Fig. 2 Adaptive control scheme

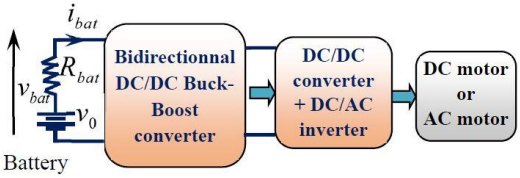

Fig. 3 Improved energy efficiency by adding a boost converter

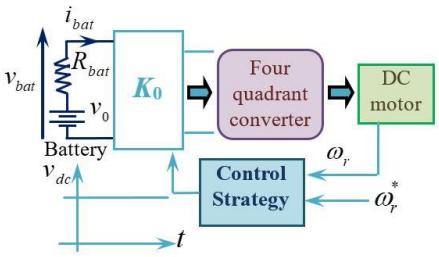

Fig. 4 Fixed amplification gain circuit

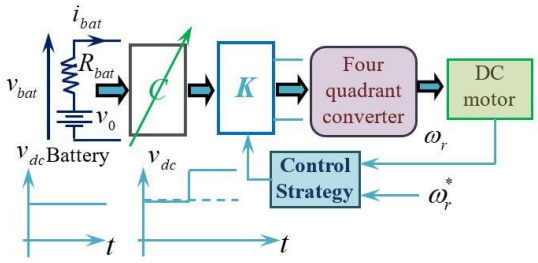

Fig. 5 Variable amplification gain circuit

voltage drop at the battery level (Fig. 2).

The third method proposed and carried out in this paper, is based on the insertion of a DC-DC boost voltage regulator, it is a less expensive solution which requires less maintenance, it makes it possible to supply the vehicle engine through the four quadrant chopper with a fixed DC voltage until the battery is completely discharged (Fig. 3).

The DC-DC boost converter is more suitable for low-power Battery Electric Vehicles (BEVs) and Plug-in Hybrid Electric Vehicles (PHEVs) because of their soft switching, noise-free operation, low switching loss and high efficiency.

However, a small-sized, reliable, parameterized, lightweight, controllable, scalable, and efficient dc-dc converter has a higher demand in automotive industries. Full bridge boost converters can also be selected for BEVs and PHEVs if galvanic isolation is required between the source and the load.

The two configurations illustrated in Figs. 4-5 respectively show the effect of a voltage regulator converter to modify the amplification gain of the four quadrant chopper in our case. The amplification gain of the four quadrant chopper of Fig. 4 can be expressed by the following equation

$$K_0 = \frac{v_{bat}}{2V_p} \quad (1)$$

Where:

K_0: is the amplifier gain of the four quadrant converter
v_{bat}: is the battery voltage
V_p: is the triangular signal of the PWM control

The insertion of a voltage regulator (C) allows modifying K_0 to a new value K which can be written in the following form

$$K = CK_0 \quad (2)$$

where:

K: is the variable amplifier gain
C: is the voltage regulator.

This configuration makes it possible to increase the maximum efficiency of the control circuit and ensure regulation under higher order conditions of the load (Fig. 5).

After having synthesized the problem of power supply and insufficient energy in an electric vehicle. Among the three methods proposed, in this paper, we are interested in carrying out the third method.

3. Modeling of the different parts of the propulsion drives structure

3.1 Modeling of the DC/DC boost converter

The boost DC-DC converter is a power converter that steps-up the input voltage while stepping down the input current (García-Rodríguez *et al*. 2018). It is a class of Switched-Mode Power Supply (SMPS) having at least one energy storage element (a capacitor, an inductor, or the two in combinations) and at least two semiconductors (a diode and a switch) as shown in Fig. 6. The same figure shows the basic structure of the power circuit of the traction chain embraced in the studied electric vehicle:

The electric motor is motorized by a four-quadrant converter (H-bridge structure) following a DC-DC bidirectional buck-boost converter which ensures the conditioning of the electrical energy during the control or recovery of the energy (Kiss *et al*. 2021).

In the bidirectional buck-boost DC-DC conversion configuration, the boost part is used to supply the traction chain with electrical energy in the direction of the motor rotation speed control, but the buck part is used to recover the power dry braking energy to the battery (reverse

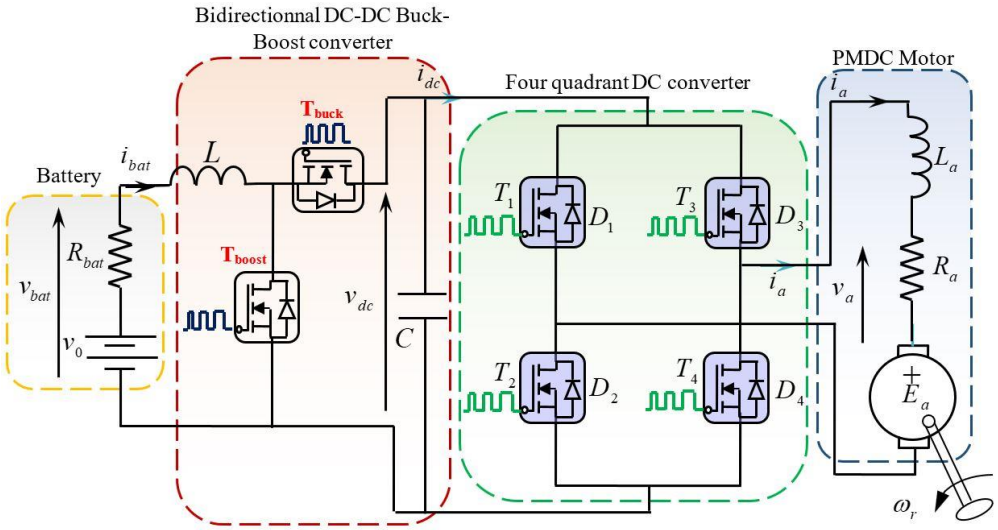

Fig. 6 The structure of the traction chain of the proposed electric vehicle

direction) or to recover the electric braking energy in the event of gravity motorization of the speed. In our experimental application, we will study the traction chain in the sense of direct speed control (circulation of electrical energy generated by the battery to the motor): Conversion mode into boost of the bidirectional buck-boost converter (Safari and Ardi 2018).

To obtain better energy efficiency in the traction chain of an electric vehicle, it is necessary to use the boost function of the bidirectional converter. This conversion mode is also used to set the input voltage of the variable speed drive to a fixed value in order to improve the regulation loop and the robustness of the Khubalkar *et al.* (2017). It is a switching power supply class (SMPS) having at least one energy storage element (a capacitor, an inductor or both in combination) and at least two bidirectional current semiconductors (T_{buck} and T_{boost}) as shown in Fig. 6.

In the boost conversion mode it is necessary to put the T_{buck} switch in (ON: open) mode permanently and the T_{boost} switch in switching mode (On or OFF: closed): If T_{boost} in (OFF), the inductance L provides energy storage in the form of a current. If T_{boost} in (ON), the energy stored in the inductance L is discharged to the capacitor C and the motorization circuit of the motor through the blocking diode D, which increases the voltage at the input of the variable speed drive to four quadrants according to the relation

$$\frac{v_{dc}}{v_{bat}} = \frac{1}{1-D} \tag{3}$$

Where:

v_{bat} is the input voltage battery [V], v_{dc} is the output voltage fed motor [V], D is the Duty Cycle of the converters.

The modeling of the DC-DC boost converter in all the operating phases can be expressed by the equation below

$$\frac{d}{dt}\begin{bmatrix} v_{dc} \\ i_{bat} \end{bmatrix} = \begin{bmatrix} -\frac{1}{RC} & \frac{1-u}{C} \\ -\frac{1-u}{L} & 0 \end{bmatrix}\begin{bmatrix} v_{dc} \\ i_{bat} \end{bmatrix} + \begin{bmatrix} 0 \\ \frac{1}{L} \end{bmatrix} v_{bat} \tag{4}$$

Where:

R: is the load resistance (equivalent of 4 quadrant DC-DC chopper + DC Motor)

Table 1 Four quadrant DC converter operating modes

State of cells switching	Direction of current flow	Phase description
T_1 operate T_1, T'_2 ON T_1 OFF → T'_2, D_4 conduct	$v_a > 0$, $i_a > 0$	In active motor phase (quadrant 1), the induced motor is powered. The stream becomes established in the armature (Mode 1).
T_2 operate T_2, D_4 ON L store energy T_2 OFF → D_1, D_4 conduct	$v_a > 0$, $i_a < 0$	In active generator phase (quadrant 2), the induced of the motor supplied power. This current may then be stored (Mode 2).
T'_1 operate T'_1, T_2 ON T'_1 OFF → T_2, D_4 conduct	$v_a < 0$, $i_a < 0$	In active motor phase (quadrant 3), the induced motor is powered but in the opposite direction. The motor then turns in the other way around (Mode 3).
T'_2 operate T'_2, D_2 ON L store energy T'_2 OFF → D_2, D_3 conduct	$v_a < 0$, $i_a > 0$	In active generator phase (quadrant 4), the induced of the motor supplied but opposed. This current can then be stored (Mode 4).

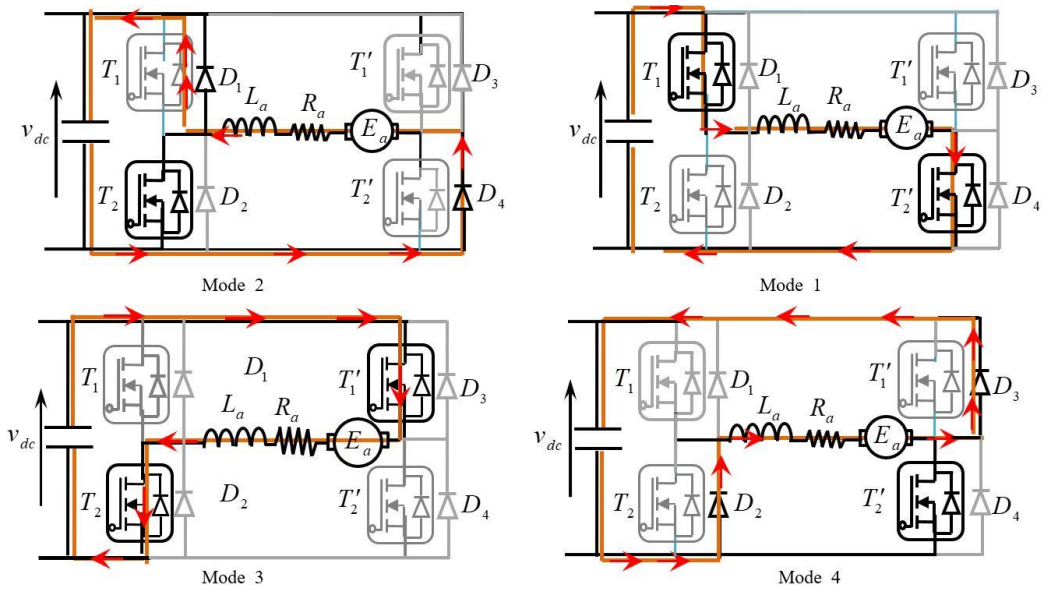

Fig. 7 Displaying of operating quadrants of DC choppers on H-bridge converter

u : is the control signal (1 or 0).

3.2 Four quadrant DC-DC converter

A DC-DC converter or DC chopper is a static device which is used to get variable DC voltage from a fixed DC voltage for variable speed drives (García-Sánchez *et al.* 2019). They are also used for DC motor control and also can run the motor in all 4 quadrant of speed torque plane. The operating principle of the four quadrant chopper is summarized in the Table 1, it operates in the four quadrants as follows (Fig. 7), we note that the symbols *T* represent the transistor and *D* the anti-parallel diode:

(1) First quadrant: in this way, positive direction of both voltage and current can be achieved and motor will rotate with forward direction. In this mode, the power flows from the supply to motor.
(2) In the second quadrant, T_1, T'_1 and T_2 switches are OFF. When the T'_2 switch is ON, the load current begins to flow by increasing through T'_2 switch and D_4 diode.
(3) Third quadrant: the voltage and current across the load are negative driving the motor in reverse direction. The motor speed can be varied by changing the Duty Cycle d of the switch T'_1.
(4) Fourth quadrant: when the switch T'_2 is turned OFF, the voltage is passed through the armature inductance and back Electro Motive Force (EMF). If the output voltage is more than source voltage, the mechanical energy is feed back to the battery as the electrical energy.

3.4 Modeling of PMDC motor

The system structure of a DC motor is depicted in Fig. 8, it is used in industrial motion control systems like the electric vehicle, electric wheelchair, etc. (Djemaï *et al.* 2011, Pisano *et al.* 2008):

The dynamic equations of a PMDC motor are modelled using Eqs. (5)-(8).

$$v_a(t) = R_a i_a(t) + L_a \frac{di_a(t)}{dt} + E_a(t) \tag{5}$$

$$T_e(t) = J\frac{d\omega_r(t)}{dt} + f\omega_r(t) + T_L(t) \tag{6}$$

$$T_e(t) = K_t i_a(t) \tag{7}$$

$$E_a(t) = K_m \omega_r(t) \tag{8}$$

Where:

R_a is the armature resistance, L_a is the winding leakage inductance, i_a is the armature current, E_a is the buck electromotive force voltage, K_m [Wb.N.m.A^{-1}] is the velocity constant determined by the flux density of the permanent magnet, ω_r [rpm] is the rotational velocity of the armature and v_a [V] is the voltage source.

Eqs. (5)-(6) can be rearranged using Eqs. (7)-(8), we obtain

$$\frac{di_a(t)}{dt} = -\frac{R_a}{L_a} i_a(t) - \frac{K_m}{L_a}\omega(t) + \frac{1}{L_a} v_a(t) \tag{9}$$

$$\frac{d\omega_r(t)}{dt} = \frac{K_m}{J} i_a(t) - \frac{f}{J}\omega_r(t) - \frac{T_L(t)}{J} \tag{10}$$

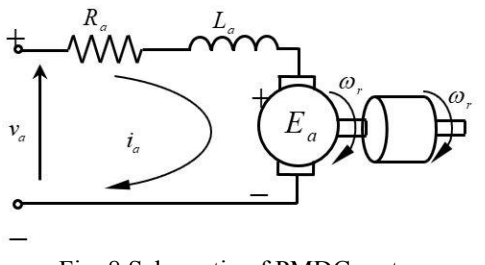

Fig. 8 Schematic of PMDC motor

Eqs. (9)-(10) represent respectively the differential equations for the armature current ($i_a(t)$) and the angular velocity ($\omega_r(t)$). These equations can be well approximated the dynamics of the PMDC-motor by the following linear time-invariant.

4. High order sliding mode control strategy

In References (Huspeka 2009, Perruquetti and Barbot 2002), the basic idea of SM control is to design first a sliding surface in state space and then the second is to design a control law direct the system state trajectory starting from any arbitrary initial state to reach the sliding surface in finite time, and finally it should come to a point where the system equilibrium state exists that is in the origin point of the phase plane. The existence, stability and hitting condition are the three factors for the stability of sliding mode control.

4.1 Design of a high sliding mode controller for DC voltage of the boost converter

The main aim of the proposed control strategy is to regulate the DC voltage of the boost converter to the desired value or to stabilize the error dynamics around zero (Wu and Lu 2019, Moussavi *et al*. 2012). The schematic circuit of the DC boost converter is presented in Fig. 9.

Let us define the variable state as follows

$$\begin{cases} x_1 = v_{dc} \\ x_2 = i_{bat} \end{cases} \tag{11}$$

From the Fig. 9, it is easy to obtain a switching model of the converter

$$\begin{cases} \dot{x}_1 = \dfrac{x_1}{RC} + \dfrac{x_2}{C}u \\ \dot{x}_2 = \dfrac{v_{bat}}{L} + \dfrac{x_1}{L}u \end{cases} \tag{12}$$

By using Euler method

$$\dot{\tilde{x}} = f(\tilde{x}) = \frac{1}{T}\left(t_{on}f^{+}(\tilde{x}) + t_{off}f^{-}(\tilde{x})\right) \tag{13}$$

Where: $T = t_{on} + t_{off}$ and: $\tilde{u} = \frac{t_{on}}{T}$

The Eq. (12) can be rewritten in the following form

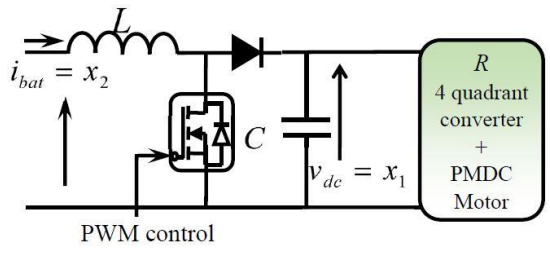

Fig. 9 Equivalent circuit of the DC boost converter for control

$$\begin{cases} \dot{\tilde{x}} = -\dfrac{\tilde{x}_1}{RC} + \dfrac{\tilde{x}_2}{C}\tilde{u} \\ \dot{\tilde{x}} = \dfrac{v_{bat}}{L} - \dfrac{\tilde{x}_1}{L}\tilde{u} \end{cases} \tag{14}$$

With: $\tilde{u} \in [0,1]$ as the Duty Cycle.

For an easier analysis, a normalized model can be obtained from Eq. (12) via the following transformation

$$\begin{cases} \xi_1 = \dfrac{x_1}{v_{bat}\sqrt{\frac{C}{L}}} \\ \xi_2 = \dfrac{x_2}{v_{bat}} \end{cases} \tag{15}$$

Which results in the system

$$\begin{cases} \sqrt{LC}\dot{\xi}_1 = 1 - u\xi_2 \\ \sqrt{LC}\dot{\xi}_2 = -\dfrac{\xi_2}{R\sqrt{\frac{C}{L}}} + u\xi_2 \end{cases} \tag{16}$$

Defining the variable

$x_{i_n} = \left(\sqrt{LC}t\right) = \xi_i(t)$ for: $i = 1, 2$

Straightforwardly, Eq. (16) yields to the normalization model

$$\begin{cases} \dot{x}_{1_n} = 1 - ux_{2_n} \\ \dot{x}_{2_n} = -\dfrac{x_{2_n}}{R_n} + ux_{1_n} \end{cases} \tag{17}$$

Where: $R_n = R\sqrt{\frac{C}{L}}$

For convenience's sake, model (17) will be rewritten drooping out the subindex *n*

$$\begin{cases} \dot{x}_1 = 1 - ux_2 \\ \dot{x}_2 = -\dfrac{x_2}{R} + ux_1 \end{cases} \tag{18}$$

Eq. (18) can be rewritten as

$$\begin{cases} \dot{x}_1 = 1 - ux_2 \\ \dot{x}_2 = -\dfrac{x_2}{R} + ux_1^* + ue_1 \end{cases} \tag{19}$$

By using a PI regulator structure

With: $e_1 = x_1 - x_1^*$

The term: x_1^* can be seen as a virtual control that considering

$$x_1^* = -\left(k_p e_2 + k_i \int_0^t e_2(s)ds\right) \tag{20}$$

The second part of the Eq. (18) takes the following form

$$\dot{x}_2 = -\frac{x_2}{R} - uk_p e_2 - uk_i \int_0^t e_2(s)ds + ue_1 \tag{21}$$

u should be designed in order to keep e_1 constant, that is

$$\dot{x}_1 = \dot{x}_1^* \tag{22}$$

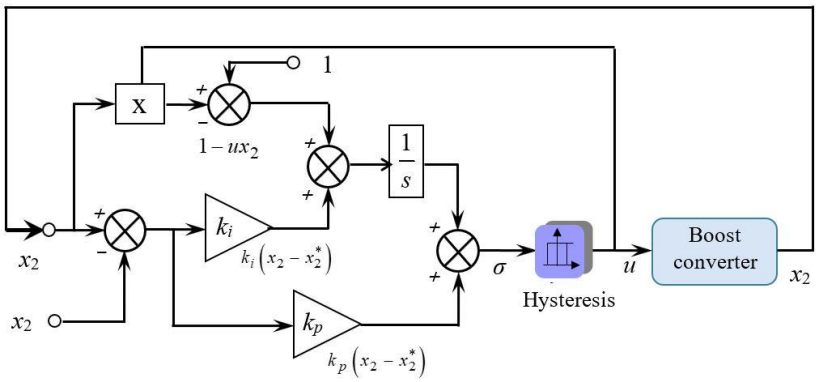

Fig. 10 The synthesis of the proposed high order sliding mode controller

From (18) and (22), the expression for u is obtained

$$u = \frac{1-\dot{x}_1^*}{x_2} = \frac{1+k_p\dot{e}_2+k_ie_2}{x_2} \tag{23}$$

If $\tilde{u}$ is the control designed for the average model, then, when the stability is assured, the system evolves in a certain surface $\sigma = 0$ and $\tilde{u}$ is the solution for u of the equation $\dot{\sigma} = 0$. (Suresh *et al*. 2019).

These ideas are applied and the Eq. (23) can be written as

$$1 - ux_2 - \dot{x}_1^* = \dot{\sigma} = 0 \tag{24}$$

By a simple integration, Eq. (24) becomes

$$\begin{aligned}\sigma &= \int_0^t \left(1-u(s)x_2(s)\right)ds - x_1^* \\ &= \int_0^t \left(1-u(s)x_2(s)\right)dt + k_pe_2 + k_i\int_0^t e_2(s)ds\end{aligned} \tag{25}$$

We note that the sliding surface $\sigma = 0$ with σ givenby Eq. (25) is dynamical, does not depend on theload and is easy to implement. The switching policy

$$u = \begin{cases}0 & \text{if } \sigma(x) < 0 \\ 1 & \text{if } \sigma(x) > 0\end{cases} \tag{26}$$

Makes the surface attractive and asymptotically stable, as the following section will show.

In practical implementation, the frequency has an upper limit set by physical limits of electronisparts. That is $h = Au$, where Au is the width of the boundary layer.

Can also be written as

$$u = \frac{1}{2}\left(1+sign(\sigma)\right) \tag{27}$$

Can be approximated by

$$u = \frac{1}{2}\left(1+hyst(\sigma,h)\right) \tag{28}$$

Fig. 10 illustrate the synthesis of the DC voltage controller.

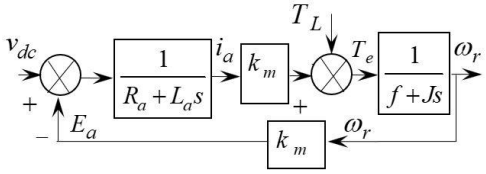

Fig. 11 The bloc diagram of a DC motor

4.2 High order sliding mode controller for mechanical rotor speed of the DC Motor

The main aim of the sliding mode controller is to regulate the rotor speed of the PMDC motor to the desired value or to stabilize the error dynamics around zero. The equivalent circuit of the DC motor to be used in this paper is seen in described in (Araria *et al*. 2020, Seeraji *et al*. 2011).

The Fig. 11, show the diagram block of the PMDC motor:

The transfer function is obtained from the block diagram of PMDC motor. Relation of the output speed ω_r to the input voltage v_{dc} with $T_L = 0$ can be expressed in the following form

$$\frac{\omega_r}{v_{dc}} = \frac{\frac{K_m}{(L_as+R_a)(Js+f)}}{1+\frac{K_m^2}{(L_as+R_a)(Js+f)}} \tag{29}$$

We get the differential equation

$$\ddot{\omega}_r = -\left(\frac{R_a}{L_a}+\frac{f}{J}\right)\dot{\omega}_r - \frac{1}{L_aJ}(R_af+K_m^2)\omega_r + \frac{K_m}{L_aJ}v_{dc} \tag{30}$$

we put

$$x_1 = \omega_r \text{ and } x_2 = \dot{x}_1 = \dot{\omega}_r$$

$$\dot{x}_2 = -\left(\frac{R_a}{L_a}+\frac{f}{J}\right)x_2 - \frac{1}{L_aJ}(R_af+K_m^2)x_1 + \frac{K_m}{L_aJ}v_{dc} \tag{31}$$

From Eqs. (30) and (31), we can get the following form

$$\begin{cases}\dot{x}_1 = 0x_1 + x_2 + 0v_{dc} \\ \dot{x}_2 = -\frac{1}{L_aJ}(R_af+K_m^2)x_1 - \left(\frac{R_a}{L_a}+\frac{f}{J}\right)x_2 + \frac{K_m}{L_aJ}v_{dc}\end{cases} \tag{32}$$

And the output: $y = x_1 = \omega_r \Rightarrow y = [0 \quad 1]\begin{bmatrix} x_1 \\ x_2 \end{bmatrix}$

Consider the space state system

$$\begin{bmatrix} \dot{x}_1 \\ \dot{x}_2 \end{bmatrix} = \begin{bmatrix} 0 & 1 \\ -\frac{1}{L_aJ}(R_af + K_m^2) & -\left(\frac{R_a}{L_a} + \frac{f}{J}\right) \end{bmatrix}\begin{bmatrix} x_1 \\ x_2 \end{bmatrix} + \begin{bmatrix} 0 \\ \frac{K_m}{L_aJ} \end{bmatrix} v_{dc} \tag{33}$$

$y = [0 \quad 1]\begin{bmatrix} x_1 \\ x_2 \end{bmatrix}$ is equivalent to the canonical form of State space

$$\begin{cases} \dot{X} = AX + Bu \\ Y = CX \end{cases} \tag{34}$$

With: $\dot{X} = \begin{bmatrix} \dot{x}_1 \\ \dot{x}_2 \end{bmatrix}$, $A = \begin{bmatrix} 0 & 1 \\ -\frac{1}{L_aJ}(R_af + K_m^2) & -\left(\frac{R_a}{L_a} + \frac{f}{J}\right) \end{bmatrix}$, $X = \begin{bmatrix} x_1 \\ x_2 \end{bmatrix}$, $B = \begin{bmatrix} 0 \\ \frac{K_m}{L_aJ} \end{bmatrix}$, $u = v_{dc}$

And: $C = [0 \quad 1]$

Control synthesis:

General equation to determine the sliding surface which ensures the convergence of a variable towards its desired value as

$$S = \dot{e} + \lambda e \tag{35}$$

The motor speed tracking error is given by the following equation

$$e = \omega_r^* - \omega_r \tag{36}$$

Or

$$e = x_r^* - x_r \tag{37}$$

Where

x_r^*: is the desired value
x_r: is the measured value

The next step would be to choose the control law (u) that will allow the error vector $(e, \dot{e})$ to reach the sliding surface.

The control law should be designed in such a way that the following condition

$$S\dot{S} < 0 \tag{38}$$

With signal control

$$u = u_s + u_{eq} \tag{39}$$

The sliding surface

$$S = \dot{e} + \lambda e \tag{4}$$

For the tracking system

$$\dot{S} = 0 \quad \Rightarrow \quad u = u_{eq} \tag{41}$$

In order to satisfy this condition, the basic discontinuous control law of sliding mode control is given by

$$u_s = Nsign(S) \tag{42}$$

With: $N > 0$

For: $\dot{S} = 0$, we'll have

$$S = \dot{e} + \lambda e \quad \Rightarrow \quad \dot{S} = \ddot{e} + \lambda\dot{e} \tag{43}$$

And

$$\begin{cases} e = \omega_r^* - \omega_r = x_r^* - x_r \\ \dot{e} = \dot{x}_r^* - \dot{x}_r = -\dot{x}_1 = -x_2 \end{cases} \tag{44}$$

And

$$\ddot{e} = -\ddot{x}_1 = -\dot{x}_2 \tag{45}$$

From the Eq. (43)

$$-\dot{x}_2 - \lambda x_2 = 0 \quad \Rightarrow \quad \dot{x}_2 + \lambda x_2 = 0 \tag{46}$$

$$-\frac{1}{L_aJ}(R_af + K_m^2)x_1 - \left(\frac{R_a}{L_a} + \frac{f}{J}\right)x_2 + \frac{K_m}{L_aJ}u + \lambda x_2 = 0 \tag{47}$$

$$\dot{S} = 0 \Rightarrow u = u_{eq} \quad \Rightarrow \quad -\frac{1}{L_aJ}(R_af + K_m^2)x_1 - \left(\frac{R_a}{L_a} + \frac{f}{J}\right)x_2 + \frac{K_m}{L_aJ}u_{eq} + \lambda x_2 = 0 \tag{48}$$

For

$$u_{eq} = \frac{L_aJ}{K_m}\left[\frac{1}{L_aJ}(R_af + K_m^2)x_1 + \left(\left(\frac{R_a}{L_a} + \frac{f}{J}\right) - \lambda\right)x_2\right] \tag{49}$$

The final control signal

$$u = u_s + u_{eq} \tag{5}$$

and too

$$u = \frac{1}{K_m}(R_af + K_m^2)x_1 + \frac{L_aJ}{K_m}\left(\left(\frac{R_a}{L_a} + \frac{f}{J}\right) - \lambda\right)x_2 - Nsign(S) \tag{51}$$

Where: λ and N are the positive real number.

The Fig. 12 illustrated the diagram block for mechanical speed control by HOSM method (Çakar and Tanyıldızı 2018).

5. The experimental setup

The control strategy has been tested experimentally. A test bench has been set up for this purpose. The test bench shown in Fig. 13 consists of: battery bank, one bidirectional DC-DC buck-boost converter (based Metal Oxide Semiconductor Field Effect Transistor (MOSFET)), one DC-DC four quadrant converter (based MOSFET), one

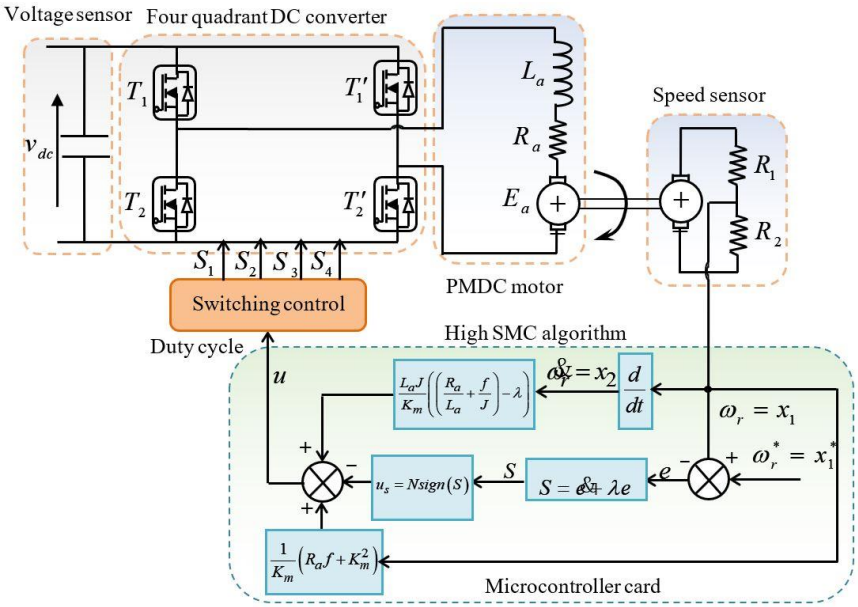

Fig. 12 High order sliding mode control of mechanical rotor speed of DC motor

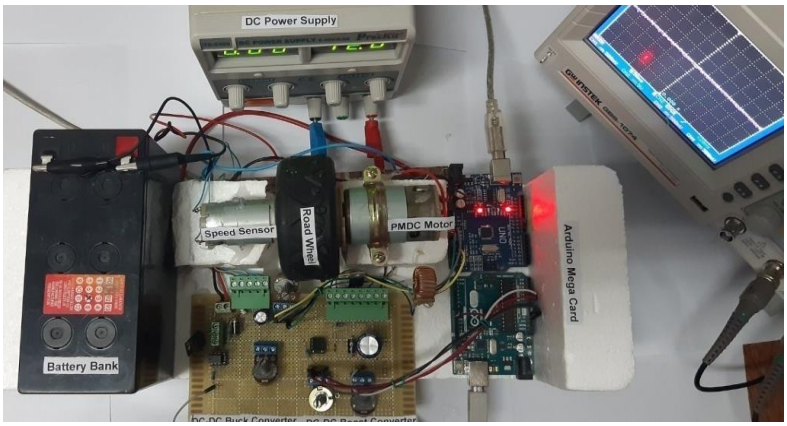

Fig. 13 Experimental setup for testing the proposed structure of electric vehicle drive

PMDC motor with rated values shown in Table 1, speed sensor for measure the rotor speed of the motor, DC voltage and current sensors, DC power supply and microcontroller card. Tables 3-4 show the parameters used in the experiment. The control frequency of the DC-DC converter and that of the inverter is 2 kHz.

The diagram in Fig. 13 shows a prototype with the aim of reproducing the behavior of the electric traction chain close to reality. On this test bench, there are two types of circuits (the power circuit and the control circuit):

The power circuit is a cascade combination of the motor (associated with the driving wheels), an electrical conversion circuit and an on-board battery. The electrical conversion circuit is formed by the association of two types of converters: A DC-DC boost converter (voltage regulator) and a four-quadrant variable speed drive (H-bridge). The H bridge is structured by four static MOSFET switches type IRFp360. In the DC-DC converter boost, the input source is of direct current type (An inductor in series with the on-board battery), the output load is of direct voltage type (capacitor in parallel with the electro-dynamic traction load), a blocking diode and a parallel static switch type MOSFET IRFp360 controlled (blocking and starting).

The variable speed drive control circuit: made up of a control card (based on two IR2112 driver circuits), an isolation card (based on four optocouplers), a real-time microcontroller card (contains the speed sliding mode program) and a measurement card (conditioning and calibration).

The DC-DC converter boost voltage regulator control circuit: consisting of an opto-optical isolation, microcontroller board (contains the DC voltage sliding mode program v_{dc}) and a voltage measurement conditioning.

A high order sliding mode control algorithm is introduced either for mechanical motor speed and direct voltage adjustment v_{dc}.

6. Experimental results and discussion

Experimental tests carried out are to assess the

efficiency and dynamic performance of the proposed power management and control approach.

The higher order sliding mode control is an expansion of the conventional sliding mode, and it can cancel the imperfection of the conventional sliding mode methodology and sustain its advantages.

Since the second-order sliding mode controller, for example, super twisting algorithm, has unsophisticated construction and requires a lesser amount of acquaintance, it is the most extensively technique that used in the higher order sliding mode methodology.

The first happens in implementation of sliding mode control in discrete-time with a digital microcontroller. The Chattering happens because the limited switching frequency due to the sampling rate, but accurate implementation of sliding mode control presupposes infinite switching frequency.

Indeed, this sort of chattering is not a problem when dealing with a system that applies discontinuous control.

DC voltage and speed control were experimentally verified on the test bench described in the previous section. Experimental tests were conducted on an electric vehicle equipped with a 68 W power PMDC motor. Numeric values of PMDC motor and the DC-DC converter parameters are giving in the appendix.

Some experimental results were provided to demonstrate the effectiveness of the proposed control technique. Tests performed with a battery voltage drop applied, v_{bat} = 7 V.

6.1 Scenario 1: Operation at nominal speed and at different speed references without DC boost

Figs. 14-15 show the performance of the motor speed, DC voltage and current obtained without DC boost. The experimental results confirm that the system loses its stability for a degraded battery voltage and no element of the conversion chain reacted to improve the situation.

In the case of a decrease in the battery voltage (to 7 Volts) caused by a failure or overconsumption, the dynamic characteristics of Fig. 14 below are obtained. Operation at low speed causes the presence of a considerable transient peak with better compliance with the order of the control in the steady state. On the other hand, in the event of an overspeed caused by the control, there is a very large static error due to the limitation of the maximum electrical power generated by the battery.

Fig. 15 shows the dynamic change in speed in the event of a decrease in the battery voltage to 7 Volts (due to failure or overconsumption). Note that the measured speed response follows its reference in low speed operation with the presence of a large transient peak at start-up. When operating at medium speed, we always notice the respect of the order of the command with a slight response time during the gradual variation of the setpoint.

When operating at high speed, we observe the collapse and total degradation of the control (due to insufficient energy and the variation in the amplification gain of the variable speed drive). Note also, the average value of the current remains approximately constant in steady state regardless of the speed variation (A constant load), except after the speed collapse (a zero current after over-variation of the speed reference and a peak current transient after cancellation of the setpoint) and vice versa speed transient: which implies disturbance, instability and incorrect operation of the control system (A command is not robust).

This makes the addition of the boost converter essential to improve the amplification gain of the 4 quadrant chopper. A series of experimental tests were carried out with the presence of the dc boost converter in the chain of the proposed electric vehicle.

6.2 Scenario 2: Rated speed operation at no load and with variable (intermittent) load

First experiment in the presence of the DC boost, the target speed is changed from 0 rpm to 1490 rpm at 1.5 s at no load applied. Fig. 16 displays the experimental result of a speed at free acceleration using the high SMC approach. Additionally, the real speed is measured and compared. It can be seen that there is a very good accordance between reference and real speed without any steady state error.

On the same Fig. 16 appears the reference and measured DC voltage evolution, the controlled voltage is not affected by the transient starting regime and the change in the reference speed set point, which explains the correct intervention of the control algorithm.

For a nominal battery voltage equal to 12 Volts, the performance shown in Fig. 16 is obtained (using the sliding

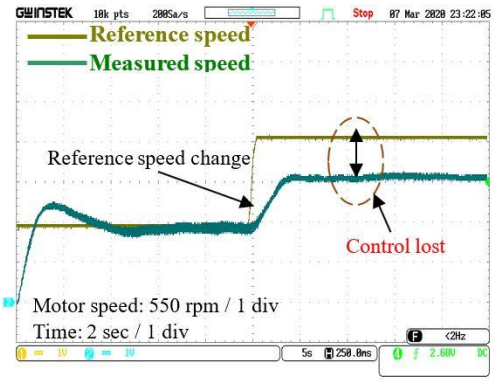

Fig. 14 Motor speed response. v_{bat} = 7 V (without DC boost)

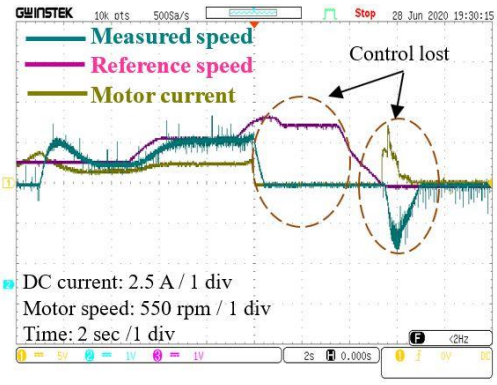

Fig. 15 Motor speed, DC voltage regulation responses and DC motor current. v_{bat} = 7 V (without DC boost)

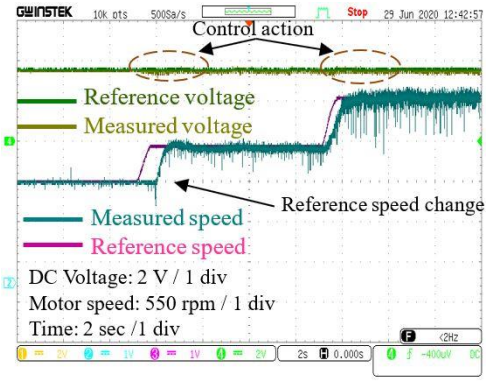

Fig. 16 Motor speed and DC voltage regulation response, motor current without load

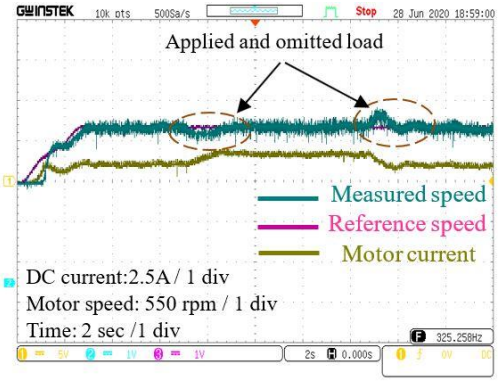

Fig. 17 Motor speed and DC voltage regulation response, motor current with a load applied

mode control). Indeed, the speed respects the order of the command regardless of the value of the setpoint with slight overshoots (or zero overshoots) in the times of variation and rapid response times (perfect dynamics).

In the same figure, we find the adjustment of the direct voltage between the output terminals of the DC-DC boost voltage regulator converter and the speed variation input to make all the parameters of the regulation chain absolutely constant (among these parameters the amplification gain of the four-quadrant converter): small (negligible) disturbances in the instants of the speed reference variation. The delay in speed response at start is justified by the current before the start value. There is also an increase in the width of the speed ripples around the setpoint (especially in the event of overspeed) due to the effect of measurement probes and the effect of the sliding mode control.

Fig. 17 shows the speed control performance where the load was applied and omitted. The measured speed coincides exactly with the reference speed even the load torque application instant.

From these results, it is shown that the proposed speed control algorithm has good performances.

Fig. 17 depicts the trajectories of motor current. It should be noting the absence of ripples and chattering of the motor current.

6.3 Scenario 3: Operation at nominal speed with application of a load torque

Fig. 18 shows the speed and the voltage control performance where the load was applied and omitted. The result clearly shows that the motor speed follows the reference speed and the error is not significant. In the same Fig. 18, the direct voltage follows its reference with a slight disturbance at the instants of application of the load torque.

6.4 Scenario 4: Operation at reference speed of staircase shape and reversing direction of rotation

A test at different reference speed levels in the form of a staircase was applied. The speed control response is illustrated in the Fig. 19. These results made the drive remain stable and this condition can be maintained indefinitely. The motor current is displayed in Fig. 19, it should be noted that the shape of the current is smooth.

The reference speed is set to 700 rpm at t = 2 s. Then the set point is changed to -700 rpm at t = 9.75 s without any load. The reversal speed response of the motor is shown in Fig. 20 at high speeds without load. It is clear that the speed response exhibits good performances at both dynamics regimes.

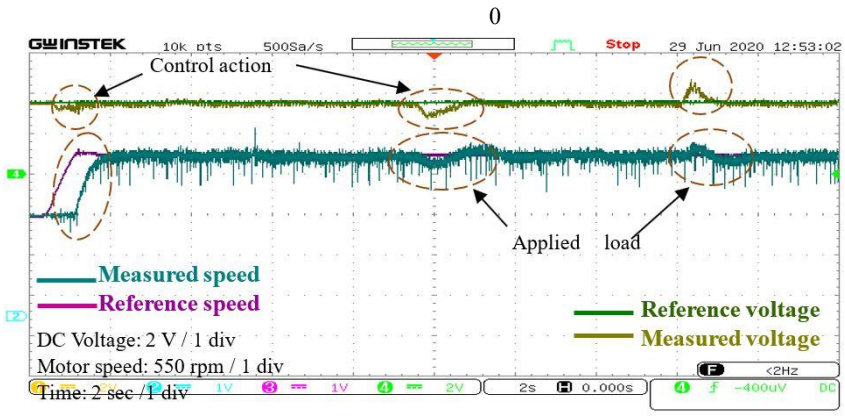

Fig. 18 The reference and measured speed, DC voltage regulation responses with applied and omitted load (rated speed operation)

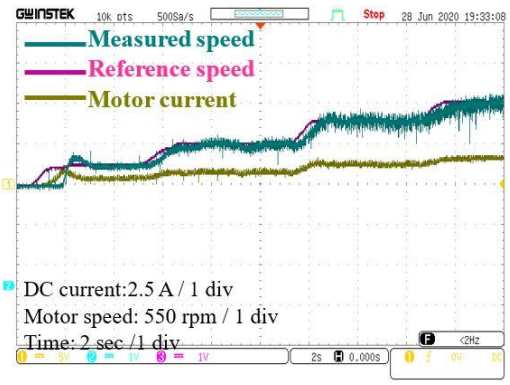

Fig. 19 Motor speed regulation and current responses (Staircase shape reference)

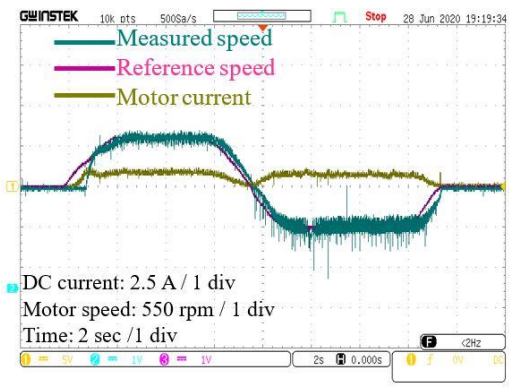

Fig. 20 Motor speed regulation and current responses (Reversal speed without load)

6.5 Scenario 5: Benchmark applied for operation for short urban journeys

A benchmark reference is applied in this test, the reference speed varies between zero and different values (different level of speed including low speed region), 1200 rpm, 2400 rpm, 3360 rpm and 4360 rpm respectively at t = 0.25 s, 0.8 s, 2.8 s and 3.8 s.

We note from the results obtained that the measured speed follows its reference perfectly with a slight overshoot (Fig. 21). Oscillations appear at the measured speed, these oscillations due to the measurement chain and the non-linearity of the electronic components used in the assembly.

This figure shows the experimental results, these results are very satisfying during the benchmark, and the speed measured is almost confused with the speed of reference. The voltage setting of this test is shown in Fig. 21, our converter kept this voltage always constant. These

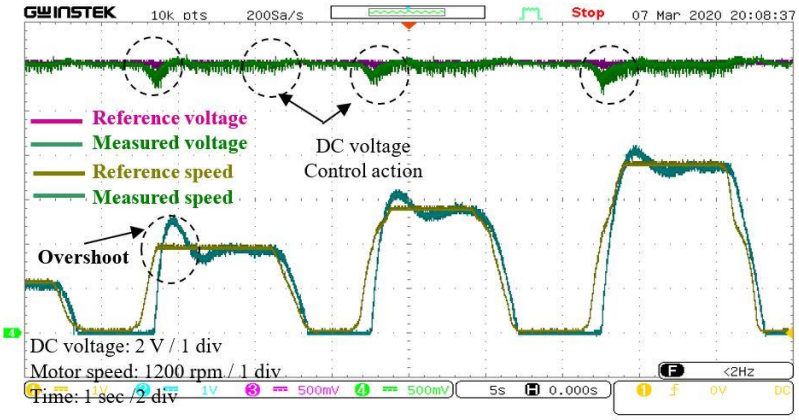

Fig. 21 Motor speed and DC voltage responses for Benchmark reference

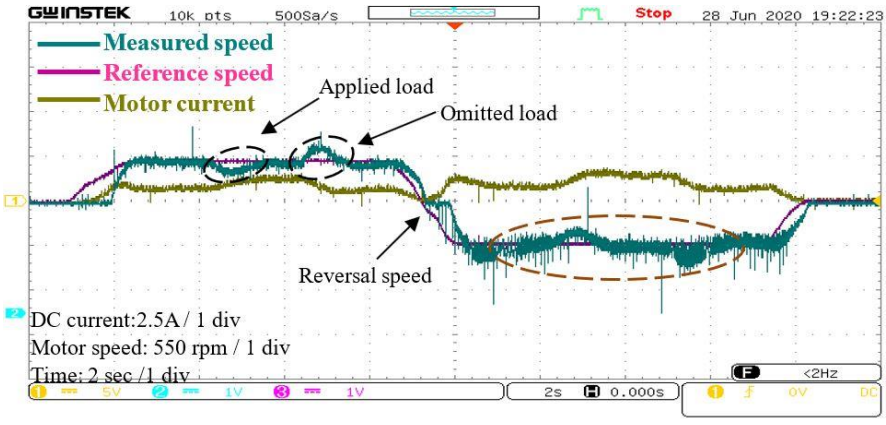

Fig. 22 Performance tracking of motor speed regulation response under rated speed operating with reversal speed and applied and omitted load, measured motor current response

Table 2 Summary of the experimental results obtained

Operation in constraint		Case of the drives	
		Without boost converter	With boost converter
Battery voltage	12 V	Good performance	Excellent performance
	7 V	Poor performance	Good performance
Speed control	12 V	Good performance	Excellent performance
	7 V	Bad performance	Good performance
Load applied	12 V	Good performance	Excellent performance
	7 V	Poor performance	Good performance
Battery fault		Bad performance	Good performance

experimental results are similar to the scenario of failure of a part of the battery, this means that the battery voltage will be degraded, according to these results, the measured DC bus voltage always follows its reference with a slight disturbance of the fault.

6.6 Scenario 6: Operation at rated speed with reversal of direction of rotation and a loaded torque is applied

The controller was tested under with the speed dependent load produced by the second DC machine. The reversal speed response of the motor is shown in Fig. 22 at high speeds under different levels of load torque. From inspection of the Fig. 22, it is possible to verify the excellent behavior of the proposed algorithm. In fact, the error on the control both of the motor speed and current are always very small (< 2%, by referring to the actual values).

Table 2 summarizes the DC voltage and motor speed performance associated with the static converters used in this practical experiment.

Excellent tracking performance was obtained no study state error and no overshoot and control performance of the drive is acceptable for load disturbance. The gotten results show the effectiveness of the proposed control scheme.

7. Conclusions

In this paper, the real-time implementation of a small electric vehicle application based on a DC boost and a four-quadrant DC converter feeding a permanent magnet DC motor to improve the dynamic and energy performance of the system under study has been presented.

A method of designing and developing a DC boost converter as a module for an electric vehicle and its control based on the higher order sliding mode technique is disclosed. The purpose of this converter is to improve the amplification gain of the four quadrant converter in the event of a large voltage drop or battery failure.

A four quadrant converter based on MOSFET was produced to drive the DC motor in all four operating configurations. Motor speed is controlled by a super twisting sliding mode control under different operating conditions, at nominal speed, under load, during rotation send reversal and also for a benchmark reference.

The proposed traction system has been subjected to several experimental tests, namely at nominal speed, under load and during the reversal of the direction of rotation with and without a boost converter. The results show the degradation of the performances without the use of a boost, on the other hand a good operation in the various constraints is obtained in the presence of the converter boost.

Among the advantages of tuning by the higher order sliding mode technique, the minimization of chattering at the levels of the signals obtained and the ease of implementing this approach. The major drawback is the variable switching.

The proposed scheme based DC boost-four quadrant converter fed a permanent magnet DC motor for electric vehicle application shows better speed control performance at different operating modes and it keeps the voltage constant for a long time in case of degradation of the performance of the battery. The system presented in this study can be easily adapted to medium and high power systems and can also be used in the wind or solar conversion chain.

Acknowledgments

The authors would like to acknowledge the financial support of the Algeria's Ministry of Higher Education and Scientific Research. This work was supported by L2GEGI laboratory at the University of Tiaret (Algeria) in collaboration with Department of automation and information, University of Cassino, Italy.

References

Adel, Z., Hamou, A.A. and Abdellatif, S. (2018), "Design of real-time PID tracking controller using Arduino Mega 2560 for a permanent magnet DC motor under real disturbances", *Proceedings of International Conference on Electrical Sciences and Technologies in Maghreb* (*CISTEM*), 1-5.

Araria, R., Negadi, K., Boudiaf, M. and Marignetti, F. (2020), "Non-linear control of DC-DC converters for battery power management in electric vehicle application", *Przegląd Elektrotechniczny*, 82-88. https://doi.org/10.15199/48.2020.03.20.

Bagheri, M.R., Mosayebi, M., Mahdian, A. and Keshavarzi, A. (2018), "Weighted sum Pareto optimization of a three dimensional passenger vehicle suspension model using NSGA-II for ride comfort and ride safety", *Smart Struct. Syst.*, **22**(4), 469-479. https://doi.org/10.12989/sss.2018.22.4.469.

Berigai Ramaiaha, A., Maurya, R. and Arya, S.R. (2018), "Bidirectional converter for electric vehicle battery charging with power quality features", *Int. Trans. Elec. Energy Syst.*, **28**(9), 1-19. https://doi.org/10.1002/etep.2589.

Bhajana, V.V.S.K., Drabek, P. and Thumma, R. (2019), "Analysis and design of a high gain non-isolated zero current switching bidirectional DC–DC converter for electric vehicles", *Automatika*: *J. Control Measur. Electro. Comput. Commun.*, **60**(1), 79-90. https://doi.org/10.1080/00051144.2019.1578915.

Çakar, O. and Tanyıldızı, A.K. (2018), "Application of moving sliding mode control for a DC motor driven four-bar mechanism", *Adv. Mech. Eng.*, **10**(3), 1-13. https://doi.org/10.1177/1687814018762184.

Djemaï, M., Busawon, K., Benmansour, K. and Marouf, A. (2011), "High-order sliding mode control of a DC motor drive via a switched controlled multi-cellular converter", *Int. J. Syst. Sci.*, **42**(11), 1869-1882. https://doi.org/10.1080/00207721.2010.545492.

Dursun, E.H., Levent, M.L., Durdu, A. and Aydoğdu, Ö. (2017), "Speed control of a variable loaded DC motor by using sliding mode and iterative learning control", *Int. J. Elec. Energy*, **5**(1), 22-28. https://doi.org/10.18178/ijoee.5.1.22-28.

García-Rodríguez, V.H., Silva-Ortigoza, R., Hernández-Márquez, E., García-Sánchez, J.R. and Taud, H. (2018), "DC/DC boost converter–inverter as driver for a DC motor: Modeling and experimental verification", *Energies*, **11**(8), 2044. https://doi.org/10.3390/en11082044..

García-Sánchez, J.R., Hernandez-Marquez, E., Ramírez-Morales, J., Marciano-Melchor, M., Marcelino-Aranda, M., Taud, H. and Silva-Ortigoza, R. (2019), "A robust differential flatness-based tracking control for the "MIMO DC/DC Boost converter-inverter–DC motor" system: Experimental results", *IEEE Access.*, **7**, 84497-84505. https://doi.org/10.1109/Access.2019.2923701.

Hernández-Márquez, E., Avila-Rea, C.A., García-Sánchez, J.R., Silva-Ortigoza, R., Silva-Ortigoza, G., Taud, H. and Marcelino-Aranda, M. (2018), "Robust tracking controller for a DC/DC Buck-Boost converter–inverter–DC motor system", *Energies*, **11**(10), 2500. https://doi.org/10.3390/en11102500.

Hoyos, F.E., Candelo-Becerra, J.E. and Rincón, A. (2021), "Zero average dynamic controller for speed control of DC motor", *Appl. Sci.*, **11**(12), 5608. https://doi.org/10.3390/app11125608.

Huspeka, J. (2009), "Second order sliding mode control of the DC motor", *Proceedings of the 17th International Conference on Process Control*, Slovakia, June.

Khubalkar, S., Junghare, A., Aware, M. and Das, S. (2017), "Modeling and control of four quadrant chopper fed DC series motor using two-degree of freedom digital fractional order PID controller", *Proceedings of 2017 IEEE Transportation Electrification Conference*, India.

Kiss, J.M., Szemes, P.T. and Aradi, P. (2021), "Sliding mode control of a servo system in LabVIEW Comparing different control methods", *Int. Rev. Appl. Sci. Eng.*, **12**(2), 201-210. https://doi.org/10.1556/1848.2021.00250.

Lavanya, M., Brisilla, R.M. and Sankaranarayanan, V. (2012), "Higher order sliding mode control of permanent magnet DC motor", *Proceedings of the 12th IEEE Workshop on Variable Structure Systems*, Mumbai, India, January.

Moussavi, S.Z., Alasvandi, M. and Javadi, S. (2012), "Speed control of permanent magnet DC motor by using combination of adaptive controller and fuzzy controller", *Int. J. Comput. Applicat.*, **52**(20), 11-15.

Nagarajan, R., Sathishkumar, S., Balasubramani, K., Boobalan, C., Naveen, S. and Sridhar, N. (2016), "Chopper fed speed control of DC motor using PI controller", *J. Elec. Electro. Eng.* (*IOSR-JEEE*), **11**(3), 65-69.

O'Brien, E.J., McGetrick, P. and González, A. (2014), "A drive-by inspection system via vehicle moving force identification", *Smart Struct. Syst.*, **13**(5), 821-848. https://doi.org/10.12989/sss.2014.13.5.821.

Perruquetti, W. and Barbot, J.P. (eds.) (2002), *Sliding Mode Control in Engineering*, Marcel Dekker, Inc., New York • Basel.

Pisano, A., Davila, A., Fridman, L. and Usai, E. (2008), "C Cascade control of PM DC drives via second-order sliding-mode technique", *IEEE Transact. Industr. Elec.*, **55**(11), 3846-3854. https://doi.org/10.1109/TIE.2008.2002715.

Safari, A. and Ardi, H. (2018), "Sliding mode control of a bidirectional buck/boost DC-DC converter with constant switching frequency", *Iran. J. Elec. Electro. Eng.*, **14**(1), 69-84. https://doi.org/10.22068/IJEEE.14.1.69.

Saleem, O., Rizwan, M., Mahmood-ul-Hasan, K. and Ahmad, M. (2020), "Performance enhancement of multivariable model reference optimal adaptive motor speed controller using error-dependent hyperbolic gain functions", *Automatika*, **61**(1), 117-131. https://doi.org/10.1080/00051144.2019.1688508.

Sankardoss, V. and Geethanjali, P. (2017), "Parameter estimation and speed control of a PMDC motor used in wheelchair", *Energy Procedia*, **117**, 345-352. https://doi.org/10.1016/j.egypro.2017.05.142.

Sankardoss, V. and, P. (2017), "Parameter estimation and speed control of a PMDC motor used in wheelchair", *Energy Procedia*, **117**, 345-352. https://doi.org/10.1016/j.egypro.2017.05.142.

Seeraji, S., Ovy, E.G., Alam, T., Zamee, A. and Al Emon, A.R. (2011), "A flexible closed loop PMDC motor speed control system for precise positioning", *Int. J. Robot. Automat.* (*IJRA*), **2**(3), 211.

Shi, X., Shi, W. and Xing, L. (2019), "Performance analysis of vehicle suspension systems with negative stiffness", *Smart Struct. Syst.*, **24**(1), 141-155. https://doi.org/10.12989/sss.2019.24.1.141.

Suresh, K., Chellammal, N., Bharatiraja, C., Sanjeevikumar, P., Blaabjerg, F. and Nielsen, J.B.H. (2019), "Cost-efficient non isolated three-port DC-DC converter for EV/HEV applications with energy storage", *Int. Trans. Elec. Energy Syst.*, **29**(10), 1-20. https://doi.org/10.1002/2050-7038.12088.

Syukriyadin, S., Syahrizal, S., Mansur, G. and Ramadhan, H.P. (2018), "Permanent magnet DC motor control by using arduino and motor drive module BTS7960", *IOP Conf. Ser: Mate. Sci. Eng.*, **352**(1), 012023. https://doi.org/10.1088/1757-899X/352/1/012023.

Tun, Z.M. and Naing, T.L. (2018), "Double loop control of H-bridge DC chopper fed permanent magnet DC motor drives using low cost hardware", *Int. J. Elec. Comput. Eng.*, **12**(11), 857-866.

Vasappa, S.V.B. and Daykumar, U. (2010), "Elimination of output voltage oscillations in DC-DC converter using PWM with PID controller", *Serbian J. Electr. Eng.*, **7**(1), 57-68.

Wu, J. and Lu, Y. (2019), "Adaptive backstepping sliding mode control for boost converter with constant power load", *IEEE Access.*, **7**, 50797-50807. https://doi.org/10.1109/ACCESS.2019.2910936.

Yang, Y.B., Li, Y.C. and Chang, K.C. (2014), "Constructing the mode shapes of a bridge from a passing vehicle: a theoretical study", *Smart Struct. Syst.*, **13**(5), 797-819. https://doi.org/10.12989/sss.2014.13.5.797.

Zhu, H.P., Ye, L., Weng, S. and Tian, W. (2018), "Damage identification of vehicle-track coupling system from dynamic responses of moving vehicles", *Smart Struct. Syst.*, **21**(5), 677-686. https://doi.org/10.12989/sss.2018.21.5.677.

CC

Appendix

Table 3 PMDC motor parameters

Components	Rated values and reference
Rated power	68.7 W
Voltage	14.4 V
Rated speed	5887 rpm
Nominal Current	1.463 A
Nominal torque	25.18 Nm
Rotor (Resistance, Inductance)	Ra = 0.8 Ω, La = 0.002 H
inertia moment	J = 0.012 kgm²/s²
viscous friction	F = 0.001 N.m.rad/s

Table 4 DC-DC Converters parameters

Components	Rated values and reference
Capacitor	140 µF
Inductance	L = 5.5 mH, r = 1.2 Ω
Resistance	100 Ω
Potentiometer	10 kΩ
MOSFET	IRF530N
Diode	UF 5408
Optocoupler	2N27

Table 5 Battery characteristics

Components	Rated values and reference
Voltage	12 V
Capacity	6 Ah